



## Exciton-dominant electroluminescence from a diode of monolayer MoS<sub>2</sub>

Yu Ye,<sup>1</sup> Ziliang Ye,<sup>1</sup> Majid Gharghi,<sup>1</sup> Hanyu Zhu,<sup>1</sup> Mervin Zhao,<sup>1,2</sup> Yuan Wang,<sup>1</sup> Xiaobo Yin,<sup>1,2</sup> and Xiang Zhang<sup>1,2,a)</sup>

<sup>1</sup>NSF Nanoscale Science and Engineering Center, University of California, 3112 Etcheverry Hall, Berkeley, California 94720, USA

<sup>2</sup>Materials Sciences Division, Lawrence Berkeley National Laboratory, 1 Cyclotron Road, Berkeley, California 94720, USA

(Received 2 April 2014; accepted 29 April 2014; published online 14 May 2014)

In two-dimensional monolayer MoS<sub>2</sub>, excitons dominate the absorption and emission properties. However, the low electroluminescent efficiency and signal-to-noise ratio limit our understanding of the excitonic behavior of electroluminescence. Here, we study the microscopic origin of the electroluminescence from a diode of monolayer MoS<sub>2</sub> fabricated on a heavily *p*-type doped silicon substrate. Direct and bound-exciton related recombination processes are identified from the electroluminescence. At a high electron-hole pair injection rate, Auger recombination of the exciton-exciton annihilation of the bound exciton emission is observed at room temperature. Moreover, the efficient electrical injection demonstrated here allows for the observation of a higher energy exciton peak of 2.255 eV in the monolayer MoS<sub>2</sub> diode, attributed to the excited exciton state of a direct-exciton transition. © 2014 AIP Publishing LLC. [<http://dx.doi.org/10.1063/1.4875959>]

The direct energy bandgap and the non-centrosymmetric lattice structure distinguish monolayer MoS<sub>2</sub> from its bulk counterpart and the widely studied monolayer graphene.<sup>1–3</sup> Extensive research efforts have been devoted to understanding its strong photoluminescence, microscopic recombination mechanisms of excitons, excessively large binding energy, and efficient control over its valley and spin degree of freedoms.<sup>4–10</sup> Prior research has suggested that excitons dominate the emission properties of these two-dimensional systems.<sup>11,12</sup> Electroluminescence, i.e., photon emission from radiative recombination of the electrically injected electrons and holes, is a reliable technique to study exciton recombination processes in monolayer MoS<sub>2</sub>, including valley and spin excitation and control. It was suggested that monolayer MoS<sub>2</sub> has potential as a two-dimensional light emitter,<sup>13</sup> in which the electroluminescence occurs through a hot carrier process and is localized in the region adjacent to the electrical contacts. However, the low electroluminescent efficiency and signal-to-noise ratio obscure the understanding of contributions from individual optical transitions. Here, we report efficient carrier injection and light emission from heterojunctions of monolayer MoS<sub>2</sub> (*n*-type) and heavily doped (*p*-type) silicon. A higher level of control over electrical carrier injection is achieved, resulting in high signal-to-noise ratio emission spectra, allowing for identification of the emissions from different optical transitions and insight into the exciton-related behaviors in electroluminescence.

In our heterojunction diodes [Fig. 1(a)], heavily *p*-doped silicon is used to inject holes into *n*-type monolayer MoS<sub>2</sub>. Highly doped *p*-type silicon on silicon oxide was microfabricated to create a step sidewall. Monolayer MoS<sub>2</sub> was placed crossing the silicon/silicon oxide step by a site-control transfer method. First, the monolayer MoS<sub>2</sub> was exfoliated on polymethyl methacrylate (PMMA). Once a monolayer MoS<sub>2</sub>

is selected, we isolate the flake by cutting the PMMA surrounding the flake using a microscale triangular knife mounted on a micromanipulator. Then, using a tungsten probe, the PMMA with the flake is picked up and moved to a precise position under a microscope. This dry transfer method allows us make a super-clean heterojunction interface. Figure 1(b) shows the schematic band structure under a forward bias; the built-in potential and applied voltage are supported by a depletion layer with abrupt boundaries. Outside the boundaries, the semiconductor is assumed to be electrically neutral. When a forward bias is applied to the heterojunction, the injection of holes from silicon across the junction can give rise to efficient radiative recombination, due to the direct band-gap of monolayer MoS<sub>2</sub>. The corresponding electroluminescence is determined by the radiative

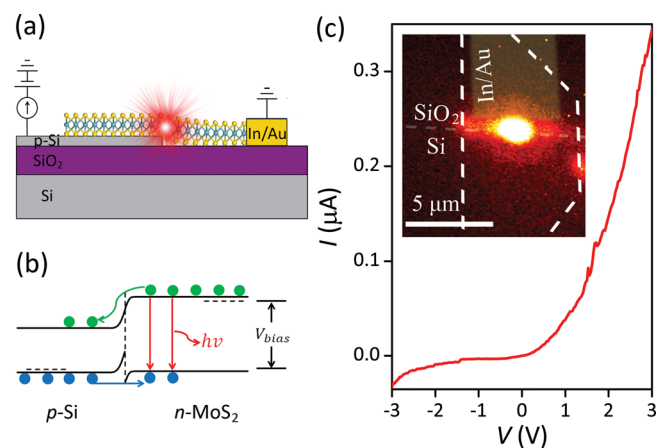


FIG. 1. (a) Schematic of the MoS<sub>2</sub>/silicon heterojunction electroluminescence device. (b) Ideal band structure of the MoS<sub>2</sub> diode under forward bias. (c) Electrical characteristics of the MoS<sub>2</sub> diode. Inset: Surface plot of the electroluminescence emission. A white light scattering image of the device is overlaid to verify that the emission is localized at the edge of the heterojunction. The white dashed line indicates the region of the monolayer MoS<sub>2</sub>. Scale bar: 5 μm.

<sup>a)</sup>Author to whom correspondence should be addressed. Electronic mail: xiang@berkeley.edu

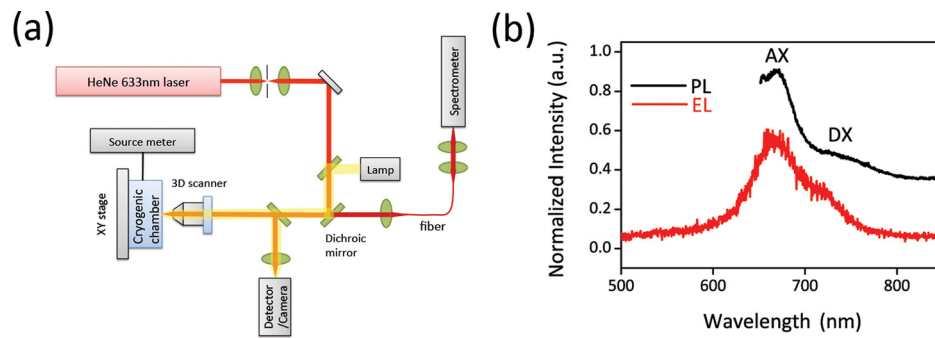


FIG. 2. (a) Schematic of our optical setup. The emission is collected through a 50x objective with an NA of 0.55. (b) Photoluminescence and electroluminescence spectra from the same device at room temperature. The electroluminescence spectrum is measured at an operating current of  $42 \mu\text{A}$ . Besides the strong direct exciton emission (labelled AX), a weaker satellite peak at lower energy is observed (labelled DX). They are attributed to the A exciton and bound exciton emission, respectively.

transitions of the monolayer  $\text{MoS}_2$ . Due to the large valence band offset between silicon and monolayer  $\text{MoS}_2$ ,<sup>14</sup> the energy band of  $\text{MoS}_2$  will bend upward under high forward bias, which is not favorable for hole-injection from silicon. In Fig. 1(c), we present the  $I$ - $V$  characteristic of a monolayer  $\text{MoS}_2$  diode, which clearly shows rectifying behavior when the voltage changes from  $-3 \text{ V}$  to  $3 \text{ V}$ . Inset of the Fig. 1(c) depicts the electroluminescent emission captured by an EM gain camera (Andor DL-604 M-#VP) from a device at a forward bias voltage with current of  $42 \mu\text{A}$  at room temperature. After superimposing a white light scattering image of the device, we find that the electroluminescence is localized at the edge of the heterojunction. By applying an in-plane bias voltage, the largest voltage drop naturally occurs across the heterojunction edge due to the semiconducting characteristics of  $\text{MoS}_2$ .<sup>15</sup> This is further confirmed by the electrostatic potential mapping by a scanning photocurrent microscopy.

To measure the photoluminescence and electroluminescence spectra, we coupled the emitted light to a fiber connected to a spectrometer (Andor Shamrock 303) as shown in Fig. 2(a). Figure 2(b) shows the room-temperature electroluminescence spectrum of monolayer  $\text{MoS}_2$  at a current of  $42 \mu\text{A}$ . The two principal luminescence features at  $667 \text{ nm}$  (labeled AX) and  $720 \text{ nm}$  (labeled DX) are associated with the A exciton and the bound exciton of monolayer  $\text{MoS}_2$ , respectively. Compared with the photoluminescence spectrum [Fig. 2(b)], the high electrical bias causes spectral broadening; electrical induced local temperature also red shifts the electroluminescence spectrum.

Figure 3(a) depicts the room-temperature electroluminescence spectra under varied currents. The electroluminescence exhibits a current threshold of about  $15 \mu\text{A}$  in this device; the two main features of the AX and DX excitation emissions are clearly observed at currents exceeding this

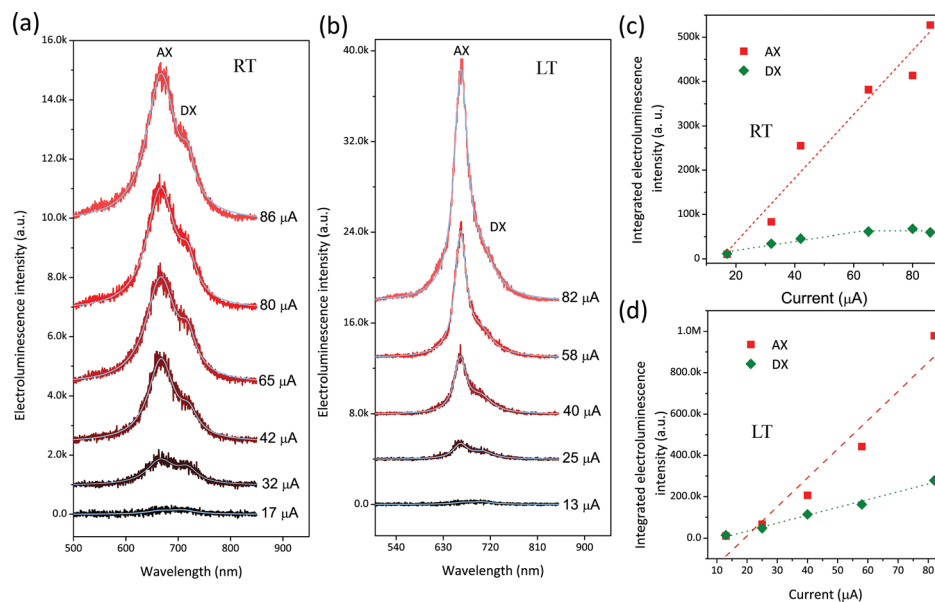


FIG. 3. (a) Room temperature electroluminescence spectra of a  $\text{MoS}_2$  diode recorded at different current levels, ranging from  $17$  to  $86 \mu\text{A}$ . The data can be well fitted with two Lorentz contributions, which are attributed to the A exciton (labelled AX) and bound exciton (labelled DX) emission. Cyan lines show the fitting results. (b) Low temperature electroluminescence spectra of the  $\text{MoS}_2$  diode shown recorded at different current levels, ranging from  $13$  to  $82 \mu\text{A}$ . The data can be well fitted with two Lorentz contributions, which are attributed to A exciton (labelled AX) and bound exciton (labelled DX) emission. Cyan lines show the fitting results. (c) Room-temperature results. Red markers: the A exciton emission (AX) shows an approximately linear increase with current. Green markers: bound exciton emission (DX). The electroluminescence saturates as the current exceed  $\sim 65 \mu\text{A}$ . The dashed lines are fitting results. (d) Red markers: the A exciton emission (AX) shows an approximately linear increase with current at low temperature. The dashed lines are fitting results. Green markers: bound exciton emission (DX) also shows an approximately linear increase with current at low temperature. The dashed lines are fitting results.

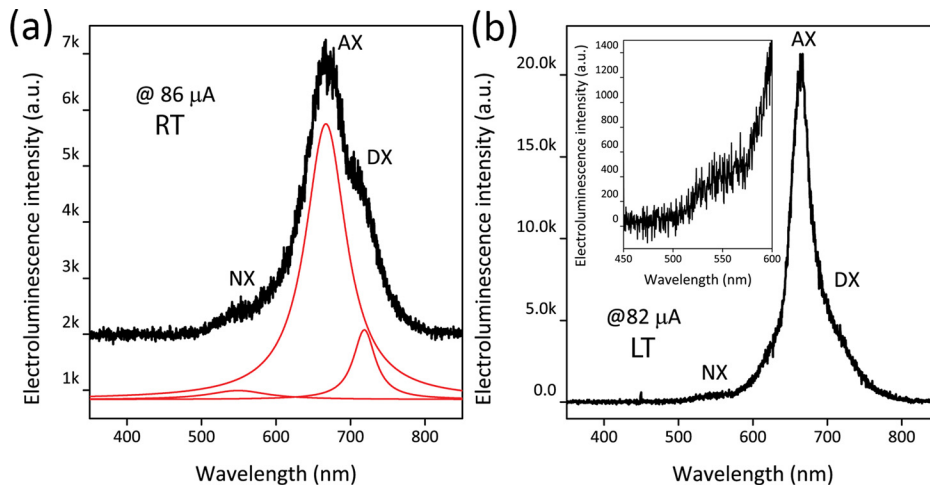


FIG. 4. (a) Room temperature electroluminescence spectrum at a current of  $82 \mu\text{A}$ . A high-energy exciton (labelled NX) feature emerges with higher exciton energy of 2.255 eV. Red curves are the Lorentz fitting result. (b) Low temperature electroluminescence spectrum at a current of  $86 \mu\text{A}$ . Inset: close-up of the NX peak region.

threshold. They are well fitted using a two-Lorentzian model. In Fig. 3(b), we present the current dependence of the AX and DX emission intensities as extracted from Fig. 3(a). The A exciton emission, AX, shows a linear dependence with increasing current. However, the bound exciton, DX, rises linearly at low currents but saturates as the current exceeds about  $65 \mu\text{A}$ . Saturation of the DX exciton emission cannot be caused by a phonon-assisted nonradiative process, as the two peaks display different current dependencies. We propose this is a different effect involving multiple exciton-exciton interactions, similar to Auger recombination, a process well documented in tightly confined carbon nanotube systems. Auger recombination may lead to rapid exciton-exciton annihilation when extra or multiple excitations are present.<sup>16–21</sup> At a low electron-hole pair injection rate, there may only be one electron-hole pair in excited monolayer MoS<sub>2</sub>. Thus, we observe linear dependence with increasing current at low injection rate. When the electron-hole pair injection rate exceeds the inverse carrier lifetime  $\tau_L^{-1}$ , more than one electron-hole pair is present in monolayer MoS<sub>2</sub>. The Auger process opens up a nonradiative recombination channel for electron-hole pair recombination. If the Auger process is sufficiently efficient, it will quickly deplete the population of electron-hole pairs. The annihilation of the electron-hole pairs comes to a stop when only a single electron-hole pair remains in the monolayer MoS<sub>2</sub>, which may lead to observed saturation of the exciton emission at sufficiently high injection current. The sudden saturation further suggests that the DX-DX annihilation lifetime  $\tau_A^{\text{DX}} \ll \tau_L$ . On the other hand, due to the absence of any noticeable AX saturation, we suspect the AX-AX annihilation lifetime  $\tau_A^{\text{AX}}$  to be longer than  $\tau_L$ .

It is well known the microscopic mechanism of optical transition is temperature dependent.<sup>12</sup> When the device temperature is cooled to 10 K, the electroluminescence resonance of AX is blue-shifted from 667 nm to 662 nm while the DX peak shifted from 720 nm to 701 nm [Fig. 3(c)]. Additionally, the full-width at half-maximum linewidth decreased down to 32 nm. The electroluminescence spectrum is very consistent with the photoluminescence spectrum at low temperature.

Again, the two main features of the AX and DX excitation emissions can be clearly read out under all the currents

above threshold [Fig. 3(c)]. In Fig. 3(d), we present the current dependence of the AX and DX emission intensities as extracted from Fig. 3(c). Both AX and DX emissions show a linear dependence with current. Surprisingly, the DX emission exhibits different current dependence behavior compared to that of room temperature. The absence of the saturation of the DX emission under a high electron-hole injection rate at low temperature is likely due to the slowing down of the Auger rate.<sup>21</sup> Past work has already shown that the lifetime of the electron-hole pair recombination in carbon nanotubes at low temperature (4.5 K) is prolonged more than one order compared to that of room temperature.<sup>19,21</sup> As the increased DX-DX annihilation lifetime  $\tau_A^{\text{DX}}$  is comparable or longer than  $\tau_L$ , the DX emission will not saturate even under high injection rate. Auger recombination of the exciton-exciton annihilation of the DX emission in monolayer MoS<sub>2</sub> system is observed in our electroluminescence. Further experimental and theoretical work will focus on measuring the timescale of the Auger recombination process.

Under a high electron-hole injection rate, a high-energy peak emerges in the electroluminescence spectra both for the room temperature [Fig. 4(a)] and low temperature [Fig. 4(b)]. We fit the electroluminescence spectrum [Fig. 4(a)] at room temperature under a current of  $86 \mu\text{A}$  with Lorentzian contributions. We find the emerged feature (labeled NX) peaks at 550 nm with energy of 2.255 eV. In low dimensional system, like monolayer MoS<sub>2</sub>, Coulomb interactions are significantly enhanced as a result of spatial confinement. Due to the large quasiparticle band gap (2.759 eV)<sup>6</sup> and the screening effect from the exciton binding<sup>22</sup> of monolayer MoS<sub>2</sub> deposited on SiO<sub>2</sub>, the emission of high energy NX may arise from the excited exciton states. Due to their low emission probabilities, the origin of the excited exciton states in MoS<sub>2</sub> system warrants further study. Recently, reports in probing the excited exciton state via linear absorption spectrum and two-photon photoluminescence excitation spectroscopy have been made. However, the emergence of high-energy NX peak in electroluminescence spectra observed in this work can shed insight into the origin of an excited exciton state and the nature of electron-orbital interactions in the MoS<sub>2</sub> system.

In conclusion, we report the electroluminescence of monolayer MoS<sub>2</sub> fabricated on a heavily *p*-type doped silicon substrate. The high signal-to-noise ratio allows for the

identification of emission from different optical transitions. Auger recombination of the exciton-exciton annihilation of bound exciton emission is observed under a high electron-hole pair injection rate at room temperature. At a high electron-hole pair injection rate, a higher energy exciton peak of 2.255 eV is observed in monolayer MoS<sub>2</sub> system. The efficient heterojunction offers a platform for fundamental investigation of the microscopic nature of the exciton recombination and may open up a pathway of controlling valley and spin excitation in MoS<sub>2</sub> diodes.

This research was supported by the U.S. Air Force Office of Scientific Research, Multidisciplinary University Research Initiative program under grant FA9550-12-1-0024 and the U.S. Department of Energy under Contract No. DE-AC02-05CH11231.

- <sup>1</sup>D. Xiao, G. Liu, W. Feng, X. Xu, and W. Yao, *Phys. Rev. Lett.* **108**, 196802 (2012).
- <sup>2</sup>A. Ramasubramaniam, *Phys. Rev. B* **86**, 115409 (2012).
- <sup>3</sup>J. Feng, X. Qian, C. Huang, and J. Li, *Nat. Photon.* **6**, 866–872 (2012).
- <sup>4</sup>A. Splendiani, L. Sun, Y. Zhang, T. Li, J. Kim, C. Chim, G. Galli, and F. Wang, *Nano Lett.* **10**, 1271–1275 (2010).
- <sup>5</sup>K. F. Mak, C. Lee, J. Hone, J. Shan, and T. F. Heinz, *Phys. Rev. Lett.* **105**, 136805 (2010).
- <sup>6</sup>T. Cheiwchanamngij and W. R. L. Lambrecht, *Phys. Rev. B* **85**, 205302 (2012).
- <sup>7</sup>T. Cao, G. Wang, W. Han, H. Ye, C. Zhu, J. Shi, Q. Niu, P. Tan, E. Wang, B. Liu, and J. Feng, *Nat. Commun.* **3**, 1–5 (2012).
- <sup>8</sup>H. Zeng, J. Dai, W. Yao, D. Xiao, and X. Cui, *Nat. Nanotechnol.* **7**, 490–493 (2012).
- <sup>9</sup>K. F. Mak, K. He, J. Shan, and T. F. Heinz, *Nat. Nanotechnol.* **7**, 494–498 (2012).
- <sup>10</sup>K. F. Mak, K. He, C. Lee, G. H. Lee, J. Hone, T. F. Heinz, and J. Shan, *Nature Mater.* **12**, 207–211 (2013).
- <sup>11</sup>H. Shi, R. Yan, S. Bertolazzi, J. Brivio, B. Gao, A. Kis, D. Jena, H. G. Xing, and L. Huang, *ACS Nano* **7**, 1072–1080 (2013).
- <sup>12</sup>T. Korn, S. Heydrich, M. Hirmer, J. Schmutzler, and C. Schüller, *Appl. Phys. Lett.* **99**, 102109 (2011).
- <sup>13</sup>R. S. Sundaram, M. Engel, A. Lombardo, R. Krupke, A. C. Ferrari, Ph. Avouris, and M. Steiner, *Nano Lett.* **13**(4), 1416–1421 (2013).
- <sup>14</sup>S. Das, H. Chen, A. V. Penumatcha, and J. Appenzeller, *Nano Lett.* **13**, 100–105 (2013).
- <sup>15</sup>T. Dufaux, M. Burghard, and K. Kern, *Nano Lett.* **12**, 2705–2709 (2012).
- <sup>16</sup>T. Muller, M. Kinoshita, M. Steiner, V. Perebeinos, A. A. Bol, D. B. Farmer, and P. Avouris, *Nat. Nanotechnol.* **5**, 27–31 (2010).
- <sup>17</sup>Y. Ma, L. Valkunas, S. L. Dexheimer, S. M. Bachilo, and G. R. Fleming, *Phys. Rev. Lett.* **94**, 157402 (2005).
- <sup>18</sup>F. Wang, Y. Wu, M. S. Hybertsen, and T. F. Heinz, *Phys. Rev. B* **73**, 245424 (2006).
- <sup>19</sup>F. Wang, G. Dukovic, E. Knoesel, L. E. Brus, and T. F. Heinz, *Phys. Rev. B* **70**, 241403(R) (2004).
- <sup>20</sup>A. Hagen, M. Steiner, M. B. Raschke, C. Lienau, T. Hertel, H. Qian, A. J. Meixner, and A. Hartschuh, *Phys. Rev. Lett.* **95**, 197401 (2005).
- <sup>21</sup>A. Högele, C. Galland, M. Winger, and A. Imamoğlu, *Phys. Rev. Lett.* **100**, 217401 (2008).
- <sup>22</sup>H. Komsa and A. V. Krashennnikov, *Phys. Rev. B* **86**, 241201(R) (2012).